Angle-dependent quasiparticle weights in correlated metals

Pouyan Ghaemi,[1] T. Senthil,[1] and P. Coleman[2]
[1]*Department of Physics, Massachusetts Institute of Technology, Cambridge, Massachusetts 02139, USA*
[2]*Department of Physics and Astronomy, Rutgers University, Piscataway, New Jersey 08854-8019, USA*
(Received 23 October 2007; revised manuscript received 21 April 2008; published 9 June 2008)

The variation in the quasiparticle weight Z on moving around the Fermi surface in correlated metals is studied theoretically. Our primary example is a heavy Fermi liquid treated within the standard hybridization mean-field theory. The most dramatic variation in the quasiparticle weight happens in situations where the hybridization vanishes along certain directions in momentum space. Such a "hybridization node" is demonstrated for a simplified model of a cerium-based cubic heavy electron metal. We show that the quasiparticle weight varies from almost unity in some directions to values approaching zero in others. This is accompanied by a similar variation in the quasiparticle effective mass. Some consequences of such hybridization nodes and the associated angle dependence are explored. Comparisons with somewhat similar phenomena in the normal metallic state of cuprate materials are discussed. A phenomenological picture of the pseudogap state in cuprates with a large Fermi surface with a severely anisotropic spectral weight is explored.

DOI: 10.1103/PhysRevB.77.245108 PACS number(s): 71.27.+a, 71.10.Ay, 71.20.Eh

I. INTRODUCTION

The normal state of cuprate materials is often described (at least empirically) as a non-Fermi-liquid metal. A remarkable feature of this metal is the presence of significant momentum-space anisotropy:[1] the extent to which Fermi-liquid theory *fails* depends strikingly on which part of a nominal Fermi surface is being probed. In optimally doped systems, quasiparticlelike peaks measured in photoemission experiments are typically much broader along the "antinodal" direction near the edges of the Brillouin zone than along the diagonal "nodal" direction. The difference is even more striking in underdoped cuprates where a pseudogap opens—apparently only near the antinodal regions, leaving behind a gapless "Fermi arc" centered at four nodal points.[2] Somewhat similar phenomena have been reported even in overdoped cuprates based on transport experiments, although the anisotropy weakens with increased doping.[3]

Theoretical understanding of such phenomena in cuprates is primitive and is hampered by the lack of a suitable framework for describing non-Fermi-liquid phenomena.[4] However, cuprates are but one example of a host of correlated metals that have been studied over the years. Fermi-liquid theory does not always fail in such metals. Motivated by the observed momentum-space anisotropy in cuprates, we therefore pose the opposite general question: does the extent to which Fermi-liquid theory *work* depend dramatically on where one is on the Fermi surface in a correlated Fermi-liquid metal? As there is a firm theoretical framework in which to discuss Fermi-liquid metals, this question can be expected to yield more easily to progress.

The most celebrated success of Fermi-liquid theory is provided by the "heavy-Fermi-liquid" state of rare-earth alloys. These have quasiparticle effective masses as high as 100–1000 times the bare electron mass and an associated small quasiparticle weight Z at the Fermi surface.[5] The main purpose of the present paper is to discuss the variation in the quasiparticle weight Z on moving around the Fermi surface. Indeed Z is a convenient measure of the extent to which Fermi-liquid theory works in a Fermi liquid. The theoretical approach we use is the standard hybridization mean-field theory for Kondo lattice models of rare-earth alloy. The variation in Z may be linked to the internal orbital structure of the Kondo singlet that forms between the local moments and the conduction electrons. This internal orbital structure derives from the symmetries of the atomic orbital occupied by the local moment and the conduction electron band it is coupled to. In the hybridization mean-field theory, this leads to angle dependence of the hybridization on going around the Fermi surface. The most dramatic variation occurs when the hybridization vanishes along some directions. Along such hybridization nodes $Z \sim o(1)$ but can become very close to zero along other directions. We demonstrate the possibility of such hybridization nodes in a simplified model appropriate for a Ce-based cubic system. Recent angle-resolved photoemission experiments[6] have begun to probe the structure of the electronic excitations of heavy Fermi liquid. We also note that recent optical transport experiments on the "1-1-5" family of materials have been interpreted in terms of momentum-dependent hybridization amplitudes.[7] This will presumably go hand in hand with angle-dependent Z. We expect that the physics described in this paper may be probed in the near future.

Very recently, experiments on $CeCoIn_5$ have reported a striking anisotropic violation of the Wiedemann–Franz law at the critical point.[8] Tanatar *et al.*[8] suggested that this might be caused by Z vanishing on some extended portions of the Fermi surface but not on others. The state we study in this paper is a Fermi-liquid state and hence does not violate the Wiedemann–Franz law. Nevertheless, the strongly angle-dependent Z that we find might provide some hints on the fundamental question of whether Z can vanish at all on some but not all portions of the Fermi surface.

Inspired by these calculations appropriate to heavy electron systems, we consider the possibility that the pseudogap regime of underdoped cuprates may actually have a large band-structure Fermi surface but with strongly angle-dependent Z. Several experimental results on underdoped cuprates are examined in this light. Such a pseudogap state has

some attractive phenomenological features—in particular, it provides one possible reconciliation between recent high-field quantum oscillation experiments[9–11] and older angle-resolved photoemission spectroscopy (ARPES) reports of gapless Fermi arcs. However, such a large-Fermi-surface Fermi-liquid state also has a number of problems with other experiments, making it unappealing as a serious theory on underdoped cuprates. A *non-Fermi-liquid* version of such a large-Fermi-surface state might perhaps resolve these difficulties, but the theoretical description of such a state remains out of reach.

II. KONDO SINGLETS WITH INTERNAL ORBITAL STRUCTURE

Heavy fermion materials are conveniently modeled as Kondo lattices, i.e., a periodic lattice of local moments coupled by magnetic exchange to a separate band of conduction electrons.[12] At low temperatures the local moments are absorbed into the Fermi sea of the metal through Kondo singlet formation. In a typical heavy electron metal, the local moments occupy atomic f orbitals. The conduction electrons derive from bands with different symmetries (s, p, or d). The Kondo singlet that forms between a local moment and a conduction electron will therefore have nontrivial internal orbital structure. In the low-temperature heavy-Fermi-liquid phase, this orbital structure leads to pronounced anisotropies between various parts of the Fermi surface. A close analogy is with the physics of unconventional superconductors where Cooper pairs with nontrivial internal orbital structure condense, leading to anisotropic superconductivity. In the heavy-Fermi-liquid case, such anisotropic effective masses are known to occur and have been discussed theoretically using a renormalized band theory approach.[13]

In the present paper we will mainly focus on the quasiparticle spectral weight Z, which is a measure of the extent to which Fermi-liquid theory works. To illustrate our point, we focus specifically on Ce-based heavy electron materials with the Ce ion in an f^1 state.[14] We also assume cubic symmetry. Such a Ce ion has, after considering the effect of spin-orbit coupling and crystal-field splitting, a low-energy Kramers doublet that couples to a separate conduction band. We treat the corresponding Kondo lattice model within the slave boson mean-field approach.[15,16] This approach is particularly well suited to describing the heavy-Fermi-liquid phase. At the mean-field level there are two bands—one derived from the f moments and the other from the conduction electrons—that are hybridized. Physically, the hybridization amplitude is a measure of the Kondo singlet formation. We show that this amplitude has strong momentum dependence coming from the symmetry of the f orbital. Thus, the true quasiparticles at the Fermi surface are angle-dependent admixtures of the f fermions and the conduction electrons. Most remarkably, we show that our simplified model naturally has directions in which the hybridization vanishes. These hybridization nodes have a number of consequences. Most importantly, it leads to a Fermi-surface structure where along the hybridization nodes the true (large) Fermi surface is contained within the original small Fermi surface of the conduction electrons. Thus, along these directions the true quasiparticle mostly has c character with weak admixture to f. Along other directions the situation is reversed. Now the physical electron spectral weight depends on the extent to which the conduction electron contributes to the quasiparticle state of the true large Fermi surface. This then leads to the dramatic variation in the quasiparticle weight discussed in Sec. I.

In passing, we note that hybridization nodes have previously been proposed in the context of theories of gapless Kondo *insulators*.[17,18] When present, such nodes have rather different effects in metallic heavy electron systems as we discuss below. Hybridization nodes are also present in toy Kondo lattice models, where each local moment is coupled to a conduction electron at a neighboring site.[19] Although such models are not directly relevant to heavy electron systems, they capture some of the same physics described in this paper.

III. ANDERSON MODEL FOR A CERIUM ION

We begin by briefly reviewing the Anderson model describing a cerium f^1 impurity in a metallic host. The f states have orbital angular momentum $l=3$ so that on including the spin, there are $2(2\times 3+1)=14$ quantum states in this orbital. Spin-orbit coupling breaks the degeneracy of this orbital into two sets of states with $J=7/2$ and $J=5/2$, where J is the total angular momentum ($J=s+l$). The $J=5/2$ states have a lower energy, and so we will concentrate on them. In a cubic environment crystal fields will further split the $J=5/2$ states into a doublet (lower-energy) state and a quadruplet (higher-energy) state. We will concentrate on the lower-energy Kramers doublet, described by $|M\rangle=|\pm\rangle$, where[14]

$$|+\rangle=\left(\frac{1}{6}\right)^{1/2}\left|J_z=-\frac{5}{2}\right\rangle-\left(\frac{5}{6}\right)^{1/2}\left|J_z=\frac{3}{2}\right\rangle,$$

$$|-\rangle=\left(\frac{1}{6}\right)^{1/2}\left|J_z=\frac{5}{2}\right\rangle-\left(\frac{5}{6}\right)^{1/2}\left|J_z=-\frac{3}{2}\right\rangle. \quad (1)$$

Now consider coupling this doublet to a band of conduction electrons $c_{k\sigma}$. We assume that the f electron in a state M can hybridize with the appropriate partial wave of the c electron also in the partial-wave state M. The coupling may therefore be modeled by the Anderson impurity Hamiltonian,[20]

$$H=\sum_{k,M}\varepsilon_{\mathbf{k}}c_{\mathbf{k}}^{\dagger}c_{\mathbf{k}}+\mu_f\sum_{M}f_M^{\dagger}f_M+U\sum_{M,M'}n_Mn_{M'}+\sum_{k,M}V_kc_{kM}^{\dagger}f_M+V_k^{*}f_M^{\dagger}c_{kM}, \quad (2)$$

with the electron partial-wave operator $c_{k,M}$, corresponding to representation in total angular momentum and magnitude k bases. The transformation between this bases and usual spin σ and vector momentum $\mathbf{k}$ bases is given by

$$c_{k,M}^{\dagger}=\sum_{\sigma}\int\frac{d\Omega_{\hat{k}}}{4\pi}c_{\mathbf{k},\sigma}^{\dagger}\langle\mathbf{k},\sigma|k,M\rangle, \quad (3)$$

where the integral is taken over all directions of the vector $\hat{k}$. For simplicity, we assume further that $V_k=V$ independent of $\mathbf{k}$.

Focusing now on the strong correlation limit of large U, we restrict the f occupation to 1, imposing the constraint

$$\sum_M f_M^\dagger f_M = 1. \tag{4}$$

The standard Schrieffer–Wolff transformation[21,22] then gives the "Kondo" effective Hamiltonian with an interaction

$$H_I = -J \sum_{k,k',M,M'} f_M^\dagger c_{k,M} c_{k',M'}^\dagger f_{M'}, \tag{5}$$

with $J = V^2 U/[\mu_f(\mu_f + U)]$. This is a Kondo type[23] interaction and describes the coupling of the fluctuating M state at the Ce site to the conduction band. Alternately, we may write

$$H_I = -J \sum_{\mathbf{k},\mathbf{k}',\sigma,\sigma',M,M'} \langle \mathbf{k}'\sigma'|k'M'\rangle\langle kM|k\sigma\rangle \times f_M^\dagger c_{\mathbf{k}\sigma} c_{\mathbf{k}',\sigma'}^\dagger f_{M'}. \tag{6}$$

IV. KONDO LATTICE MODEL

We now generalize the description of a single Ce impurity ion in Sec. III to a lattice of Ce ions. We first introduce the operators $f_{M,\mathbf{R}}$ for the local moments at site $\mathbf{R}$ of the lattice. The generalization of the Kondo interaction H_I is clearly

$$H_K = -J \sum_{\mathbf{R}} \sum_{\mathbf{k},\sigma,\mathbf{k}',\sigma',M,M'} \langle \mathbf{k}',\sigma'|k',M',\mathbf{R}\rangle\langle k,M,\mathbf{R}|\mathbf{k},\sigma\rangle \times f_{\mathbf{R},M}^\dagger c_{\mathbf{k},\sigma} c_{\mathbf{k}',\sigma'}^\dagger f_{\mathbf{R},M'}, \tag{7}$$

where $|k,M,R\rangle$ is a c-electron partial wave centered at site $\mathbf{R}$. We have

$$|k,M,\mathbf{R}\rangle = e^{i\hat{\mathbf{P}}\cdot\mathbf{R}}|k,M\rangle, \tag{8}$$

where $\hat{\mathbf{P}}$ is the momentum operator (generator of translation) and $|k,M\rangle$ is a partial wave centered at the origin. Thus, we get

$$\langle \mathbf{k},\sigma|k,M,\mathbf{R}\rangle = \langle \mathbf{k},\sigma|e^{i\hat{\mathbf{P}}\cdot\mathbf{R}}|k,M\rangle = e^{i\mathbf{k}\cdot\mathbf{R}}\langle \mathbf{k},\sigma|k,M\rangle \tag{9}$$

since $\langle \mathbf{k},\sigma|$ is momentum eigenstate. With Fourier transforming the $c_{\mathbf{k}}$ electrons back to real space ($c_{\mathbf{k},\sigma} = \Sigma_{\mathbf{r}} e^{i\mathbf{k}\cdot\mathbf{r}} c_{\mathbf{r},\sigma}$), we get

$$H_K = -J \sum_{\mathbf{R}} \sum_{\mathbf{r},\mathbf{r}',M,M'} f_{M,\mathbf{R}}^\dagger \left[\sum_{\mathbf{k},\sigma} \langle k,M|\mathbf{k},\sigma\rangle e^{i\mathbf{k}\cdot(\mathbf{r}-\mathbf{R})} c_{\mathbf{r},\sigma} \right] \times \left[\sum_{\mathbf{k}',\sigma'} \langle \mathbf{K}',\sigma'|k',M'\rangle e^{-i\mathbf{k}'\cdot(\mathbf{r}'-R)} c_{\mathbf{r}',\sigma'}^\dagger \right] f_{M',\mathbf{R}}. \tag{10}$$

It is convenient now to define real-space operators

$$\Gamma_{\mathbf{r},\mathbf{R},M} = \sum_{\mathbf{k},\sigma} \langle k,M|\mathbf{k},\sigma\rangle e^{i\mathbf{k}\cdot(\mathbf{r}-\mathbf{R})} c_{\mathbf{r},\sigma}, \tag{11}$$

which are a mixture of spin-up and spin-down electrons. In terms of these real-space operators, the Kondo interaction assumes the simple form

$$H_K = -J \sum_{\mathbf{R}} \sum_{\mathbf{r},\mathbf{r}'} \sum_{M,M'} f_{M,\mathbf{R}}^\dagger \Gamma_{\mathbf{r},\mathbf{R},M} \Gamma_{\mathbf{r}',\mathbf{R},M'}^\dagger f_{M',\mathbf{R}'}. \tag{12}$$

The full Kondo lattice model then takes the form

$$H = H_c + H_K, \tag{13}$$

$$H_c = \sum_{\mathbf{k},\sigma} \varepsilon_{\mathbf{k}} c_{\mathbf{k},\sigma}^\dagger c_{\mathbf{k},\sigma}, \tag{14}$$

together with the constraints

$$\sum_M f_{M,\mathbf{R}}^\dagger f_{M,\mathbf{R}} = 1, \tag{15}$$

at each site $\mathbf{R}$. Note that due to this constraint, it is no longer appropriate to think of the f operators as describing physical electrons. Rather, at this stage they should be viewed as neutral fermions that carry spin alone. As is well known, this representation is redundant and introduces an extra U(1) gauge structure associated with the freedom to change the phase of f independently at each site.

V. SLAVE BOSON MEAN-FIELD THEORY

We now discuss the Fermi-liquid phases described by this Kondo lattice model within the slave boson mean-field approximation. In simpler Kondo lattice models this technique correctly captures the essential physics of the Fermi-liquid state.[16] In the mean field we impose the constraint in Eq. (15) on average with a chemical potential μ_f for the f fermions and replace the Kondo interaction by a self-consistently determined hybridization between the c and f operators. The mean-field Hamiltonian reads

$$H_{\mathrm{MF}} = \sum_{\mathbf{k}\sigma} \varepsilon_{\mathbf{k}} c_{\mathbf{k}\sigma}^\dagger c_{\mathbf{k}\sigma} + \mu_f \sum_{M\mathbf{R}} f_{M,\mathbf{R}}^\dagger f_{M,\mathbf{R}} + b \sum_{M\mathbf{R}} \left(f_{M\mathbf{R}}^\dagger \sum_{\mathbf{r}} \Gamma_{\mathbf{r}\mathbf{R}M} + \mathrm{H.c.} \right). \tag{16}$$

The mean-field parameters μ_f, b must be determined self-consistently through the equations

$$1 = \sum_M \langle f_{M,\mathbf{R}}^\dagger f_{M,\mathbf{R}}\rangle, \tag{17}$$

$$b = J\langle \sum_M f_{M\mathbf{R}}^\dagger \sum_{\mathbf{r}} \Gamma_{\mathbf{r}\mathbf{R}M}\rangle. \tag{18}$$

Note that we have chosen b to be real in this mean field. Parenthetically, we note that a nonzero mean-field hybridization parameter b should really be viewed as a Higgs condensate for the U(1) gauge structure introduced when we represent the spins in terms of the f fields. In this Higgs phase the internal gauge charge of the f fermions is screened by the condensate, and the resulting screened gauge neutral object has the same quantum numbers as the electron. This structure of the low-energy electrons manifests itself as a small electron quasiparticle weight at the heavy electron Fermi surface.

To diagonalize this mean-field Hamiltonian, we go to momentum space. We write $f_{M,\mathbf{R}} = \Sigma_{\mathbf{q}} e^{-i\mathbf{q}\cdot\mathbf{R}} f_{M,\mathbf{q}}$ and put in the original form of Γ operators in terms of c. The hybridization term then becomes

$$H_{\mathrm{MF}} = b\sum_{\mathbf{R},\mathbf{r}}\sum_{\mathbf{q}} e^{i\mathbf{q}\cdot\mathbf{R}} f^{\dagger}_{M,\mathbf{q}} \sum_{\mathbf{k},\sigma} \langle k,M|\mathbf{k},\sigma\rangle e^{i\mathbf{k}\cdot(\mathbf{r}-\mathbf{R})} c_{\mathbf{r},\sigma} + \mathrm{H.c.}$$
$$= b\sum_{\mathbf{q},\mathbf{k},\sigma}\left(\sum_{\mathbf{R}} e^{i(\mathbf{q}-\mathbf{k})\cdot\mathbf{R}}\right) f^{\dagger}_{M,q}\langle k,M|\mathbf{k},\sigma\rangle$$
$$\times\left(\sum_{\mathbf{r}} e^{i\mathbf{k}\cdot\mathbf{r}} c_{\mathbf{r},\sigma}\right) + \mathrm{H.c.}$$
$$= b\sum_{\mathbf{k}} \langle k,M|\mathbf{k},\sigma\rangle f^{\dagger}_{M,\mathbf{k}} c_{k,\sigma} + \mathrm{H.c.} \quad (19)$$

Thus, the momentum dependence of the hybridization is captured through the $\langle \mathbf{k},\sigma|k,M\rangle$ matrix element, which we calculate in the Appendix.

We define the four-component field Ψ_k as

$$\Psi_k = \begin{bmatrix} c_{\mathbf{k}\uparrow} \\ c_{\mathbf{k}\downarrow} \\ f_{k,1} \\ f_{k,2} \end{bmatrix},$$

in terms of which the Hamiltonian becomes

$$H_{\mathrm{MF}} = \sum_{\mathbf{k}} \Psi^{\dagger}_{\mathbf{k}} \begin{bmatrix} \varepsilon_{\mathbf{k}}\mathbf{I} & bM(\mathbf{k}) \\ bM^{\dagger}(\mathbf{k}) & \mu_f\mathbf{I} \end{bmatrix} \Psi_{\mathbf{k}}. \quad (20)$$

Here $M(\mathbf{k})$ is a 2×2 matrix given by

$$M(\mathbf{k}) = \begin{bmatrix} B(\mathbf{k}) & A^*(\mathbf{k}) \\ A(\mathbf{k}) & -B^*(\mathbf{k}) \end{bmatrix}. \quad (21)$$

The functions $A(\mathbf{k})$ and $B(\mathbf{k})$ are defined in the Appendix.

Now we look for operators $\gamma_i(\mathbf{k})$ that satisfy $[H_{\mathrm{MF}}, \gamma^{\dagger}_i(\mathbf{k})] = \lambda_i(\mathbf{k})\gamma^{\dagger}_i(\mathbf{k})$, in terms of which H^{MF} is diagonal,

$$H_{\mathrm{MF}} = \sum_{\mathbf{k},i} \lambda_i(\mathbf{k})\gamma^{\dagger}_i(\mathbf{k})\gamma_i(\mathbf{k}). \quad (22)$$

If we express $\gamma_i(\mathbf{k})$ as

$$\gamma_i(\mathbf{k}) = u^1_i(\mathbf{k})c_{\mathbf{k}\uparrow} + u^2_i(\mathbf{k})c_{\mathbf{k}\downarrow} + u^3_i(\mathbf{k})f_{\mathbf{k}1} + u^4_i(\mathbf{k})f_{\mathbf{k}2}, \quad (23)$$

where the coefficients $u^{\alpha}_i(\mathbf{k})$ are determined through the eigenvalue equation

$$\begin{bmatrix} \varepsilon_{\mathbf{k}}\mathbf{I} & bM(\mathbf{k}) \\ bM^{\dagger}(\mathbf{k}) & \mu_f\mathbf{I} \end{bmatrix} \begin{bmatrix} u^1_i(\mathbf{k}) \\ u^2_i(\mathbf{k}) \\ u^3_i(\mathbf{k}) \\ u^4_i(\mathbf{k}) \end{bmatrix} = \lambda_i(\mathbf{k}) \begin{bmatrix} u^1_i(\mathbf{k}) \\ u^2_i(\mathbf{k}) \\ u^3_i(\mathbf{k}) \\ u^4_i(\mathbf{k}) \end{bmatrix}. \quad (24)$$

From this we get the four eigenstates and the corresponding dispersion of four bands,

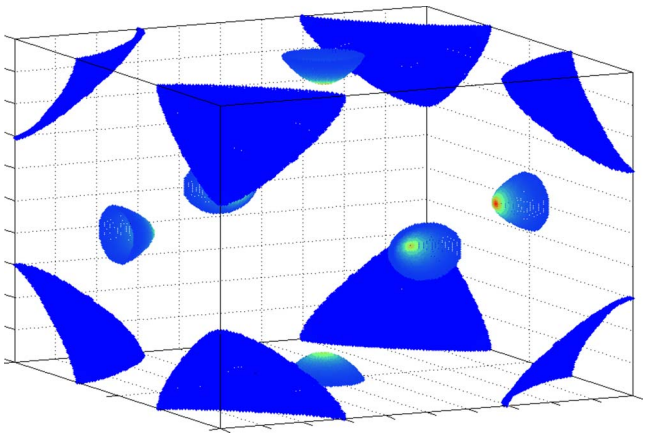

FIG. 1. (Color online) Z on the Fermi surface. Red denotes larger Z close to 1 and blue denotes Z close to zero. Red points are along the (0,0,1), (0,1,0), and (0,0,1) directions.

$$\lambda_1(\mathbf{k}) = \lambda_2(\mathbf{k}) = \frac{\varepsilon_{\mathbf{k}} + \mu_f}{2} - \sqrt{\left(\frac{\varepsilon_{\mathbf{k}} - \mu_f}{2}\right)^2 + b^2(|A(\Omega_{\mathbf{k}})|^2 + |B(\Omega_{\mathbf{k}})|^2)},$$

$$\lambda_3(\mathbf{k}) = \lambda_4(\mathbf{k}) = \frac{\varepsilon_{\mathbf{k}} + \mu_f}{2} + \sqrt{\left(\frac{\varepsilon_{\mathbf{k}} - \mu_f}{2}\right)^2 + b^2(|A(\Omega_{\mathbf{k}})|^2 + |B(\Omega_{\mathbf{k}})|^2)}.$$

At each $\mathbf{k}$ obviously we have $\lambda_1(\mathbf{k}) = \lambda_2(\mathbf{k}) \le \lambda_3(\mathbf{k}) = \lambda_4(\mathbf{k})$, so we have two sets of doubly degenerate bands. The degeneracy is a consequence of time reversal and inversion symmetries which have been assumed in the original model.

Let us assume that there are n_c conduction electrons per unit cell with $n_c < 1$. Once combined with a single f fermion per unit cell, we then need to fill these bands up to the Fermi energy to give a total particle number of $1+n_c$ per unit cell. Only states in the lower bands λ_1 and λ_2 are electron filled, and the Fermi surface always exists in these two bands. Clearly, the Fermi surface is large in that its volume counts both the conduction electrons and the f fermions. The shape of the Fermi surface corresponding to our simple model is shown in Fig. 1.

We note that the hybridization matrix $bM(\vec{k})$ vanishes along (100) and symmetry related directions (see the Appendix). These hybridization nodes lead to striking Fermi-surface anisotropies, as discussed in detail below. For now we note that along these nodal directions the Fermi surface coincides within the original *small* conduction electron Fermi surface. To see this, consider the spectrum of the partially occupied band. It is obvious that $\lambda(\mathbf{k}) = \lambda_1(\mathbf{k}) < \frac{\varepsilon_{\mathbf{k}}+\mu_f}{2} - \left|\frac{\varepsilon_{\mathbf{k}}-\mu_f}{2}\right|$. On the other hand, $\frac{\varepsilon_{\mathbf{k}}+\mu_f}{2} - \left|\frac{\varepsilon_{\mathbf{k}}-\mu_f}{2}\right| = \min\{\varepsilon_{\mathbf{k}}, \mu_f\}$ so that for all $\mathbf{k}$, $\lambda(\mathbf{k}) \le \mu_f$ [the equality only holds for the points where $b(\mathbf{k}) = b^2(|A(\Omega_{\mathbf{k}})|^2 + |B(\Omega_{\mathbf{k}})|^2) = 0$]. Thus, for $n_c < 1$, $E_f < \mu_f$. Now if we consider points on the Fermi surface where $b(\mathbf{k})$ vanishes, again for such points $\lambda(\mathbf{k})$ is equal to either μ_f for points where $\varepsilon_{\mathbf{k}} > \mu_f$ and $\varepsilon_{\mathbf{k}}$ for points where

$\varepsilon_{\mathbf{k}} < \mu_f$. Since $E_f < \mu_f$, for such points we have $\lambda(\mathbf{k}) = \varepsilon_{\mathbf{k}}$; so the Fermi surface coincides with the small Fermi sea of conduction electrons at the points where $b(\mathbf{k}) = 0$. Thus, along the nodal directions of the hybridization, the quasiparticles at the Fermi surface are almost entirely composed of conduction electrons. However, on moving away from these nodal directions, the quasiparticles quickly acquire an almost complete f character with a weak conduction electron admixture.

VI. IMPLICATIONS FOR PHOTOEMISSION EXPERIMENTS

The anisotropic hybridization leads, as discussed below, to anisotropic quasiparticle spectral weight. This can be probed by ARPES. We begin with a general discussion of the physical electron Green's function in Kondo lattice systems.

Let us start with Anderson model given in Eq. (2). In ARPES by interaction with a light beam, electrons are extracted from the sample. These electrons in principle could be extracted form any of the two bands [see Eq. (2)]. However, processes where the f occupation is changed cost a large energy in the strong correlation limit. On the other hand, processes where the removed f electron is replaced by tunneling of a c electron into the unoccupied f site can occur at order (V/U) and will have matrix elements in the low-energy Kondo subspace. To discuss this physics, let us start from a single Anderson impurity and consider the operator $\psi_{\mathbf{k},\sigma}$ that corresponds to extracting an electron with momentum $\mathbf{k}$ and spin σ out of the sample,

$$\psi_{\mathbf{k},\sigma} = c_{\mathbf{k},\sigma} + \sum_M \langle \mathbf{k},\sigma|M\rangle f_M. \tag{25}$$

In the strong correlation limit, we need to perform the Schrieffer–Wolff transformation for this operator. Below we use an equivalent alternate procedure. We first consider the ground state. In the limit of infinite U it consists of a half-filled f orbital coexisting with a conduction band filled up to the Fermi energy. We name this state $|g_0\rangle$. In the limit of large but finite U to first order in V/U the ground state becomes

$$|g_1\rangle = |g_0\rangle + \sum_{n,M,\mathbf{k},\sigma} |n\rangle \frac{\langle n|V(f_M^\dagger c_{\mathbf{k},\sigma} + c_{\mathbf{k},\sigma}^\dagger f_M)|g_0\rangle}{U}, \tag{26}$$

where, for simplicity, we have assumed that the energy to add, or remove, an f electron is U. Here $|n\rangle$ denote the first excited states. To a good approximation, the state vector in the second term is given by $(f_M^\dagger c_{\mathbf{k},\sigma} + c_{\mathbf{k},\sigma}^\dagger f_M)|g_0\rangle$. Now when we annihilate an electron by acting with ψ on $|g_1\rangle$ state, only final states which lie within the manifold of states with single f occupancy at the impurity site will contribute to the photoemission intensity at low energy. There are two such states, one corresponding to the action of c on the $|g_0\rangle$ component of the ground state and the other corresponding to the action of f on the second term in $|g_1\rangle$ (i.e., on the $f^\dagger c|g_0\rangle$ term). The net action of $\psi_{\mathbf{k},\sigma}$ on $|g_0\rangle$ is then

$$\psi_{\mathbf{k},\sigma} \sim c_{\mathbf{k},\sigma} + (V/U) \sum_{\mathbf{k}',\sigma',M',M} \langle k',M'|\mathbf{k}',\sigma'\rangle \times \langle \mathbf{k},\sigma|k,M\rangle f_{M'}^\dagger c_{\mathbf{k}',\sigma'} f_M. \tag{27}$$

The first term corresponds to the knocking off of an electron from the c band and the second term corresponds to the first-order process, where an electron from an f orbital is knocked off and an electron from the c band replaces it. Now for a lattice of impurities, we should consider processes where f electrons from different sites are knocked out,

$$\psi_{\mathbf{k},\sigma} \sim c_{\mathbf{k},\sigma} + (V/U) \sum_{\mathbf{R}} \sum_{\mathbf{k}',\sigma',M',M} \langle k',M',\mathbf{R}|\mathbf{k}',\sigma'\rangle \times \langle \mathbf{k},\sigma|k,M,\mathbf{R}\rangle f_{M',\mathbf{R}}^\dagger c_{\mathbf{k}',\sigma'} f_{M,\mathbf{R}}. \tag{28}$$

It is convenient to re-express this in real space. The procedure is the same as the one we followed in Sec. V,

$$\sum_{\mathbf{R}} \sum_{\mathbf{k}',\sigma',M'} \langle k',M',\mathbf{R}|\mathbf{k}',\sigma'\rangle \langle \mathbf{k},\sigma|k,M,\mathbf{R}\rangle f_{M',\mathbf{R}}^\dagger c_{\mathbf{k}',\sigma'} f_{M,\mathbf{R}} = \sum_{\mathbf{R}} \sum_{\mathbf{k}',\sigma',M'} \langle k',M'|\mathbf{k}',\sigma'\rangle e^{i\mathbf{k}'\cdot(\mathbf{r}-\mathbf{R})} f_{M',\mathbf{R}}^\dagger c_{\mathbf{r},\sigma'},$$

$$\langle \mathbf{k},\sigma|k,M\rangle e^{i\mathbf{k}\cdot\mathbf{R}} f_{M,\mathbf{R}} = \sum_{\mathbf{R}} \sum_{M'} f_{M',\mathbf{R}}^\dagger \left[\sum_{\mathbf{k}',\sigma} \langle k',M'|\mathbf{k}',\sigma'\rangle e^{i\mathbf{k}'\cdot(\mathbf{r}-\mathbf{R})} c_{\mathbf{k}',\sigma'} \right],$$

$$\sum_M e^{i\mathbf{k}\cdot\mathbf{R}} f_{M,\mathbf{R}} = \sum_{\mathbf{R}} \sum_{M'} f_{M',\mathbf{R}}^\dagger \Gamma_{\mathbf{r},\mathbf{R},M'} \sum_M \langle \mathbf{k},\sigma|k,M\rangle f_{M,\mathbf{R}}. \tag{29}$$

Within the slave boson mean-field approximation, we replace the product $f^\dagger c$ (or, equivalently, $f^\dagger \Gamma$) term in the second term by its average to get

$$\psi_{\mathbf{k},\sigma} \sim c_{\mathbf{k},\sigma} + (b/V) \sum_M \langle \mathbf{k},\sigma|k,M\rangle f_M. \tag{30}$$

The ARPES intensity may now be calculated from the Green's function of this ψ operator. Its trace is given by

$$\mathrm{Tr}[G_{\sigma,\sigma'}(k,i\omega_\nu)] = \int_0^\beta d\tau e^{i\omega_\nu \tau} \langle T_\tau [\psi_\uparrow(k,\tau)\psi_\uparrow^\dagger(k,0) + \psi_\downarrow(k,\tau)\psi_\downarrow^\dagger(k,0)]\rangle, \tag{31}$$

where the expectation value is taken in the ground state. From Eq. (30) it is obvious that this Green's function consists of four different terms. For this calculation, we need to have c_σ and f_M operators, in terms of γ operators. To make this calculation more transparent, it is useful to introduce the unitary matrix U as

$$U = \begin{bmatrix} u_1^1 & u_1^2 & u_1^3 & u_1^4 \\ u_2^1 & u_2^2 & u_2^3 & u_2^4 \\ u_3^1 & u_3^2 & u_3^3 & u_3^4 \\ u_4^1 & u_4^2 & u_4^3 & u_4^4 \end{bmatrix}, \tag{32}$$

where

$$\begin{bmatrix} \gamma^1 \\ \gamma^2 \\ \gamma^3 \\ \gamma^4 \end{bmatrix} = U \begin{bmatrix} c_\uparrow \\ c_\downarrow \\ f_1 \\ f_2 \end{bmatrix}. \tag{33}$$

Here the $\mathbf{k}$ index is suppressed for notational convenience. Inverting, we get

$$c_\uparrow^\dagger = u_1^1 \gamma_1^\dagger + u_2^1 \gamma_2^\dagger + u_3^1 \gamma_3^\dagger + u_4^1 \gamma_4^\dagger, \tag{34}$$

$$c_\downarrow^\dagger = u_1^2 \gamma_1^\dagger + u_2^2 \gamma_2^\dagger + u_3^2 \gamma_3^\dagger + u_4^2 \gamma_4^\dagger, \tag{35}$$

$$f_1^\dagger = u_1^3 \gamma_1^\dagger + u_2^3 \gamma_2^\dagger + u_3^3 \gamma_3^\dagger + u_4^3 \gamma_4^\dagger, \tag{36}$$

$$f_2^\dagger = u_1^4 \gamma_1^\dagger + u_2^4 \gamma_2^\dagger + u_3^4 \gamma_3^\dagger + u_4^4 \gamma_4^\dagger. \tag{37}$$

Using this result, we can expand the imaginary part of the trace of Green's function to obtain the zero-temperature spectral function. This has four terms corresponding to the operator combinations $cc^\dagger$,$ff^\dagger$, $fc^\dagger$, and $cf^\dagger$. Let us calculate them one by one. The $cc^\dagger$ term is

$$A_{cc}(\mathbf{k},\omega) = [|u_1^1(\mathbf{k})|^2 + |u_1^2(\mathbf{k})|^2]\delta[\lambda_1(\mathbf{k}) - \omega] + [|u_2^1(\mathbf{k})|^2 + |u_2^2(\mathbf{k})|^2]\delta[\lambda_2(\mathbf{k}) - \omega]. \tag{38}$$

We then get the following form for the quasiparticle residue on the Fermi surface:

$$Z_{cc}[\,\mathbf{k}|\lambda_2(\mathbf{k}) = E_f] = |u_2^1(\mathbf{k})|^2 + |u_2^2(\mathbf{k})|^2 = \frac{b(\mathbf{k})^2}{b(\mathbf{k})^2 + \left[\frac{\varepsilon(\mathbf{k})-\mu_f}{2} + \sqrt{\left(\frac{\varepsilon(\mathbf{k})-\mu_f}{2}\right)^2 + b(\mathbf{k})^2}\right]^2}. \tag{39}$$

Now for ff term (noting $u_1^3 = u_2^4 = 0$) we have

$$A_{ff}(\mathbf{k},\omega) = \left[\frac{b(\mathbf{k})}{V}\right]^2 |u_4^1(\mathbf{k})|^2 \delta[\lambda_1(\mathbf{k}) - \omega] + \left[\frac{b(\mathbf{k})}{V}\right]^2 |u_2^3(\mathbf{k})|^2 \delta[\lambda_2(\mathbf{k}) - \omega]. \tag{40}$$

This gives the residue

$$Z_{ff}[\,\mathbf{k}|\lambda_2(\mathbf{k}) = E_f] = \frac{\left\{\frac{\varepsilon(\mathbf{k})-\mu_f}{2} + \sqrt{\left[\frac{\varepsilon(\mathbf{k})-\mu_f}{2}\right]^2 b(\mathbf{k})^2}\right\}^2}{b(\mathbf{k})^2 + \left\{\frac{\varepsilon(\mathbf{k})-\mu_f}{2} + \sqrt{\left[\frac{\varepsilon(\mathbf{k})-\mu_f}{2}\right]^2 + b(\mathbf{k})^2}\right\}^2} \left\{\frac{b(\mathbf{k})}{V}\right\}^2. \tag{41}$$

The last contribution will be

$$Z_{cf}[\,\mathbf{k}|\lambda_2(\mathbf{k}) = E_f] = -\frac{2(b^2/V)\left\{\frac{\varepsilon(\mathbf{k})-\mu_f}{2} + \sqrt{\left[\frac{\varepsilon(\mathbf{k})-\mu_f}{2}\right]^2 + b(\mathbf{k})^2}\right\}}{b(\mathbf{k})^2 + \left\{\frac{\varepsilon(\mathbf{k})-\mu_f}{2} + \sqrt{\left[\frac{\varepsilon(\mathbf{k})-\mu_f}{2}\right]^2 + b(\mathbf{k})^2}\right\}^2} \times \Re[A^2(\Omega_\mathbf{k}) + B^2(\Omega_\mathbf{k})], \tag{42}$$

where $b(\mathbf{k}) = b\sqrt{|A(\Omega_\mathbf{k})|^2 + |B(\Omega_\mathbf{k})|^2}$. In Fig. 1 we have also indicated the total residue Z_{total}, which is the sum of these three contributions.

Using the fact that $|b(\mathbf{k})|$ is small, we can investigate the behavior of Z_{total} at least for the points where $|b(\mathbf{k})| \ll |\varepsilon(\mathbf{k}) - \mu_f|$. For such points we see that whenever $\epsilon_\mathbf{k} > \mu_f$, the dominant term (of order b^2/V^2) is Z_{ff} and it varies since $b(\mathbf{k})$ is angle dependent. On the other hand, when $\epsilon_\mathbf{k} < \mu_f$, the dominant contribution is Z_{cc}, which is of order one. This information could be summarized in the following form:

$$Z[\,\mathbf{k}|\lambda_2(\mathbf{k}) = E_f] = b^2 \frac{h(\mathbf{k})}{[\varepsilon(\mathbf{k}) - \mu_f]^2}\Theta[\varepsilon(\mathbf{k}) - \mu_f] + \Theta[\mu_f - \varepsilon(\mathbf{k})], \tag{43}$$

where $h(\mathbf{k})$ is given by

$$h(\mathbf{k}) = [|A^2(\Omega_\mathbf{k})| + |B^2(\Omega_\mathbf{k})|]\{1 + [\varepsilon(\mathbf{k}) - \mu]^2/V^2\} - 2\Re[A^2(\Omega_\mathbf{k}) + B^2(\Omega_\mathbf{k})][\varepsilon(\mathbf{k}) - \mu]/V. \tag{44}$$

A key result of this calculation is that for the points where $\varepsilon(\mathbf{k}) > \mu_f$, Z is small and of order $\frac{b(\mathbf{k})^2}{[\varepsilon(\mathbf{k})-\mu_f]^2}$; this quantity varies by about 20% due to the angle-dependent $b(\mathbf{k})$. However, for the points where $\mu_f > \varepsilon(\mathbf{k})$, the quasiparticle residue will be of order one and will exhibit no strong variations. The small region in the middle of the Fermi surface in Fig. 1 with $Z \sim 1$ corresponds to these points. These regions are centered along (100) and symmetry related directions. As discussed in Sec. V, the hybridization matrix has nodes in these special directions and the corresponding quasiparticles are essentially conduction electrons with $Z \sim 1$. On the other hand, farther away from these nodal directions, the quasiparticles develop f character and $Z \sim o(b^2)$ along these other directions.

There is thus a dramatic anisotropy in Z on moving around the Fermi surface. We note that ARPES experiments will naturally be able to resolve the quasiparticle peak along high-Z directions. However, a low-resolution ARPES study may not be able to resolve well the small-Z quasiparticles at all and may incorrectly conclude that the Fermi surface consists only of finite open ended pieces.

VII. MOMENTUM-DEPENDENT EFFECTIVE MASS

It is well known that the effective mass m^* in a heavy fermion system can be very anisotropic on the Fermi surface. How do these anisotropies correlate with the anisotropic Z? It is precisely the combination $Z \times m^*$ that determines the *tunneling* density of states. It is therefore also interesting to look at $m^*(\mathbf{k})$ variations over the Fermi surface. The effective mass can be calculated by taking the second derivative of energy with respect to momentum in the direction perpendicular to the Fermi surface, i.e., $\frac{\partial^2 \lambda_2(\mathbf{k})}{\partial k_\perp^2}$:

$$1/[m^*(\mathbf{k})] = 1/2m_e^*\left[1 - \frac{\frac{\varepsilon_\mathbf{k}-\mu_f}{2}}{\sqrt{\left(\frac{\varepsilon_\mathbf{k}-\mu_f}{2}\right)^2 + |b(\mathbf{k})|^2}} + \frac{b^2(\varepsilon_\mathbf{k}-\mu_f)f(\mathbf{k})}{\left[\left(\frac{\varepsilon_\mathbf{k}-\mu_f}{2}\right)^2 + |b(\mathbf{k})|^2\right]^{3/2}}\right] \approx 1/m_e^*\left\{\Theta[\mu_f - \varepsilon(\mathbf{k})] + \frac{b^2}{(\varepsilon_\mathbf{k}-\mu_f)^2}g(\mathbf{k})\right\}, \quad (45)$$

where m_e^* is the free-electron effective mass ($1/m_e^* = \frac{\partial^2 \varepsilon_\mathbf{k}}{\partial k_\perp^2}$). In the last step we used the approximation $|\varepsilon_\mathbf{k} - \mu_f| \gg |b(\mathbf{k})|$. $f(\mathbf{k})$ and $g(\mathbf{k})$ are dimensionless functions of $\mathbf{k}$, where $g(\mathbf{k}) = 2\ \mathrm{sgn}(\varepsilon_\mathbf{k} - \mu_f)[4f(\mathbf{k}) + |A(\Omega_\mathbf{k})|^2 + |B(\Omega_\mathbf{k})|^2]$ [numerical calculations show no $\mathbf{k}$ point where $g(\mathbf{k})$ vanishes]. Inverting this, we get

$$m^*(\mathbf{k}) \approx m_e^*\left\{\Theta[\mu_f - \varepsilon(\mathbf{k})] + \Theta[\varepsilon(\mathbf{k}) - \mu_f]\frac{(\varepsilon_\mathbf{k}-\mu_f)^2}{g(\mathbf{k})b^2}\right\}. \quad (46)$$

We see a similar behavior for $Z(\mathbf{k})$. Again, for points with $\varepsilon_\mathbf{k} > \mu_f$ we have quasiparticles with a large effective mass, but for $\varepsilon_\mathbf{k} < \mu_f$ quasiparticles are free-electron types and have an effective mass corresponding to a small conduction electron's effective mass. We see that we have large effective masses at the points where Z is small. Thus, variations in effective mass are indeed correlated with variations in $1/Z$. The approximate invariance of the product $Z(\mathbf{k})m^*(\mathbf{k})$ is a momentum-space variant of the Langreth theorem, which states that the single particle density of states in the Anderson impurity model is an adiabatic invariant, independent of the strength of the interaction.[24,25]

This is interesting since it shows us that the strong angle-dependent anisotropy does not apparently have a large observable consequence on ordinary tunneling measurements. However, it may possibly show up in the amplitude of the Friedel oscillations of the tunneling conductance around an impurity and may therefore be accessible through Fourier transform scanning tunneling spectroscopy.

VIII. UNDERDOPED CUPRATES: PSEUDOGAPS AND FERMI ARCS IN A LARGE-FERMI-SURFACE METAL?

We now compare the phenomena described to observations on the normal state of cuprate materials. As discussed above in the heavy fermion context there are portions of the Fermi surface where $Z \sim o(1)$, and ARPES experiments may conclude that the Fermi surface consists of open ended pieces. This is strongly reminiscent of the Fermi arc phenomena reported by ARPES in the pseudogap regime of underdoped cuprates. It is tempting therefore to imagine that a similar mechanism is operational in cuprates. More specifically, is it possible that underdoped cuprates actually have a large band-structure-like Fermi surface but the Z is $o(1)$ only along the observed Fermi arcs and becomes very small away from it so that those portions are not easily observed? The antinodal pseudogap itself must then be associated with a gap in the incoherent part of the electron spectrum with the gapless coherent part not resolved due to the smallness of Z.

In considering this question, we first observe that in the heavy fermion system, the smallness of Z goes hand in hand with the largeness of the effective mass. More generally, the effective mass is not directly related to Z (it is only in cases where the electron self-energy is momentum independent that Z determines the mass renormalization). So phenomenologically, we need to first suppose that the small-Z antinodal regions do not have mass enhancement. Such a Fermi-liquid state for the pseudogap regime has some attractive features. Consider first the gapless Fermi arcs. Several popular theories attempt to view the arcs as part of a true Fermi surface which consists of small closed hole pockets whose *back* portions are not observed in ARPES due to a small Z. However, the observed Fermi arc coincides with band-structure Fermi surface and shows no tendency to bend away into a closed hole pocket. In contrast, in the state discussed above the true Fermi surface is simply the band-structure one but the antinodal sections would be unobservable due to a small Z.

Consider next recent observations of quantum oscillations at high fields and low temperatures in some underdoped cuprates.[9,10] The oscillation frequency seems consistent with a small Fermi pocket. A key issue is to reconcile this with the Fermi arcs reported in photoemission, and a few different ideas have been proposed.[26,27] An interesting feature of the high-field experiments is a negative Hall constant, which has been interpreted as evidence for an *electron* pocket.[28] Recently, Millis and Norman[29] proposed that the oscillations and negative Hall constant should be with a 1/8 filling antiphase stripe order, which folds the band-structure Fermi surface to create a pocket. One issue with the proposal is that the electron pocket is near the edges of the full Brillouin zone—precisely the region where a big pseudogap is seen by ARPES in zero field in the normal state above T_c. For the theory in Ref. 29 to apply, it is apparently necessary that the 60 T fields used in the quantum oscillation experiment wipe out the pseudogap.[30] This may seem unnatural but is not prohibited. This difficulty is overcome in the large-Fermi-surface pseudogap envisaged in this section. A low-temperature 1/8 antiphase stripe instability arising from that state will retain all the same transport properties as that in the theory in Ref. 29. This is because the smallness of Z does not affect transport phenomena. On the other hand, the ARPES pseudogap (which in this state is the gap of the incoherent part of the spectrum) will survive intact. Thus, this kind of large-Fermi-surface state provides a possible route to a reconciliation between the quantum oscillation and ARPES experiments.

However, a number of difficulties exist with the idea that the pseudogap state has a large-Fermi-surface state with strong angle-dependent Z. First, the density of states as measured by thermodynamic measurements actually decreases on entering the pseudogap state by cooling. This requires that the effective mass at the antinodal regions is *suppressed* (rather than enhanced) in the pseudogap state, which is rather

unnatural. Besides, such behavior should signal an increase in the Drude weight in optical transport in the pseudogap state, which is not seen. Finally, this is also inconsistent with the scaling of the superfluid density with the density of doped holes.

In light of these difficulties, it seems unlikely that a Fermi-liquid state with a large Fermi surface of the kind discussed here is a serious candidate for the pseudogap state. These difficulties may perhaps be overcome by a non-Fermi-liquid version which retains the large Fermi surface and the strong variation in the low-energy spectral density. However, a description of such a state does not currently exist.

IX. DISCUSSION

The most interesting aspect of our work is the possibility of large variations in the quasiparticle weight (and, concomitantly, the effective mass) on moving around the Fermi surface. This anisotropy is linked to the internal orbital structure of the Kondo resonance, derived from the f symmetry of the orbitals occupied by the local moments. In the hybridization mean-field theory, the most dramatic variation occurs when there are hybridization nodes, i.e., directions along which the hybridization vanishes. We have demonstrated the possibility of these nodes in a simple model of a Ce-based cubic heavy fermion system with cubic symmetry. Hybridization nodes lead to the possibility that some portions of the large Fermi surface are actually contained within the original small Fermi surface of the conduction electrons. In those regions the quasiparticles essentially have a c-electron character with very little admixture to the f fermions. The quasiparticle weight is correspondingly large (of order 1). The opposite is true in other portions where the quasiparticles mostly have an f character and have small Z. This then leads to a strong angle dependence of the quasiparticle weight.

Real heavy electron materials have much more complicated band structures than in the simplified model considered here. Nevertheless, there exists in general the possibility of hybridization nodes, which will greatly affect their low-temperature physics. Consider, for instance, heavy electron superconductivity. At least in some cases the superconductivity may be driven by formation of singlet bonds between neighboring local moments due to Ruderman–Kittel–Kasuya–Yosida interactions. In combination with Kondo hybridization, this leads to superconductivity. Formally, the singlet formation may be described as $\langle ff\rangle$ pairing, while the Kondo hybridization has nonzero $\langle c^{\dagger}f\rangle$. This then leads to nonzero $\langle cc\rangle$, i.e., superconducting order.[31,32] If the hybridization has nodes, then this will lead to extra nodes in the physical superconducting order parameter over and above any nodes inherited from the singlet bond $\langle ff\rangle$ amplitude.[33]

The large variation in Z also has potential implications on current thinking on the nature of the quantum critical point between the heavy Fermi liquid and the antiferromagnetic metal. It has been suggested that this transition is accompanied by the loss of Kondo screening, resulting in a reconstruction of the Fermi surface.[34–36] Such a reconstruction presumably requires Z to vanish through out the large Fermi surface on approaching the transition from the paramagnetic side. For a discussion on Z vanishing at the heavy fermion quantum critical points, see Ref. 37. The variation in Z described in this paper raises the question of whether the manner in which Z vanishes also varies around the Fermi surface.

We also explored the possibility that the pseudogap state of underdoped cuprates may be a large-Fermi-surface Fermi-liquid state with a strongly angle-dependent Z. While such a picture has some very appealing features, it has enough difficulties with experiments that it is unlikely to directly be a relevant theory of the pseudogap state.

ACKNOWLEDGMENTS

We thank A. J. Millis, P. A. Lee, and L. Taillefer for useful discussions. P.C. was supported by NSF Grant No. DMR 0605935.

APPENDIX: CALCULATION OF MATRIX ELEMENT

To calculate $\langle \mathbf{k},\sigma|k,M\rangle$, we use the known overlap of $|\mathbf{k},\sigma\rangle$ and $|k,J_z\rangle$ (Ref. 38) for $l=3$,

$$\langle \mathbf{k},\sigma|k,J_z\rangle = 4\pi[\alpha_{J_z} Y_3^{J_z+1/2}(\Omega_{\mathbf{k}})\delta_{\sigma,-1/2} + \beta_{J_z} Y_3^{J_z-1/2}(\Omega_{\mathbf{k}})\delta_{\sigma,1/2}], \tag{A1}$$

where $Y_l^m(\Omega_{\mathbf{k}})$ are associated Legendre functions and $\alpha_{J_z}=[(7+2J_z)/14]^{1/2}$ and $\beta_{J_z}=[(7-2J_z)/14]^{1/2}$ are Clebsch–Gordan coefficients.[38] Now using the forms given in Eq. (A1), we get the following for the two orbital states:

$$\langle \mathbf{k},\sigma|\mathbf{1}\rangle = \frac{1}{\sqrt{6}}\left[\frac{1}{\sqrt{7}}Y_3^{-2}(\Omega_{\mathbf{k}})\delta_{\sigma,-1/2} + \sqrt{\frac{6}{7}}Y_3^{-3}(\Omega_{\mathbf{k}})\delta_{\sigma,1/2}\right] - \sqrt{\frac{5}{6}}\left[\sqrt{\frac{5}{7}}Y_3^{2}(\Omega_{\mathbf{k}})\delta_{\sigma,-1/2} + \sqrt{\frac{2}{7}}Y_3^{1}(\Omega_{\mathbf{k}})\delta_{\sigma,1/2}\right],$$

$$\langle \mathbf{k},\sigma|\mathbf{2}\rangle = \frac{1}{\sqrt{6}}\left[\sqrt{\frac{6}{7}}Y_3^{3}(\Omega_{\mathbf{k}})\delta_{\sigma,-1/2} + \frac{1}{\sqrt{7}}Y_3^{2}(\Omega_{\mathbf{k}})\delta_{\sigma,1/2}\right] - \sqrt{\frac{5}{6}}\left[\sqrt{\frac{2}{7}}Y_3^{-1}(\Omega_{\mathbf{k}})\delta_{\sigma,-1/2} + \sqrt{\frac{5}{7}}Y_3^{-2}(\Omega_{\mathbf{k}})\delta_{\sigma,1/2}\right].$$

It is more convenient to work with a simplified version of these relations, as

$$\langle \mathbf{k},\sigma|\mathbf{1}\rangle = \frac{1}{\sqrt{42}}[Y_3^{-2}(\Omega_{\mathbf{k}}) - 5Y_3^{2}(\Omega_{\mathbf{k}})]\delta_{\sigma,-1/2} + \frac{1}{\sqrt{42}}[\sqrt{6}Y_3^{-3}(\Omega_{\mathbf{k}}) - \sqrt{10}Y_3^{1}(\Omega_{\mathbf{k}})]\delta_{\sigma,1/2},$$

$$\langle \mathbf{k},\sigma|\mathbf{2}\rangle = \frac{1}{\sqrt{42}}[\sqrt{6}Y_3^3(\Omega_\mathbf{k}) - \sqrt{10}Y_3^{-1}(\Omega_\mathbf{k})]\delta_{\sigma,-1/2} + \frac{1}{\sqrt{42}}[Y_3^2(\Omega_\mathbf{k}) - 5Y_3^{-2}(\Omega_\mathbf{k})]\delta_{\sigma,1/2}.$$

If we introduce new functions $A(\Omega_\mathbf{k})$ and $B(\Omega_\mathbf{k})$,

$$\langle \mathbf{k},\sigma|\mathbf{1}\rangle = A(\Omega_\mathbf{k})\delta_{\sigma,-1/2} + B(\Omega_\mathbf{k})\delta_{\sigma,1/2},$$

$$\langle \mathbf{k},\sigma|\mathbf{2}\rangle = -B^*(\Omega_\mathbf{k})\delta_{\sigma,-1/2} + A^*(\Omega_\mathbf{k})\delta_{\sigma,1/2}, \quad \text{(A2)}$$

where $A(\Omega_\mathbf{k}) = \frac{4\pi}{\sqrt{42}}[Y_3^{-2}(\Omega_\mathbf{k}) - 5Y_3^2(\Omega_\mathbf{k})]$ and $B(\Omega_\mathbf{k}) = \frac{4\pi}{\sqrt{42}}[\sqrt{6}Y_3^{-3}(\Omega_\mathbf{k}) - \sqrt{10}Y_3^1(\Omega_\mathbf{k})]$.

[1] X. J. Zhou *et al.*, Phys. Rev. Lett. **92**, 187001 (2004).
[2] M. R. Norman, H. Ding, M. Randeria, T. Y. J. Campuzano, T. Takeuchi, T. Takahashi, T. Michiku, K. Kad-owaki, P. Guptasarma, and D. Hinks, Nature (London) **392**, 157 (1998).
[3] M. Abdel-Jawad, M. P. Kennett, L. Balicas, A. Carrington, A. P. MacKenzie, R. H. McKenzie, and N. E. Hussey, Nat. Phys. **2**, 821 (2006).
[4] Some interesting results on the momentum-space anisotropy have been obtained in cluster dynamical mean-field theory studies [B. Kyung, S. S. Kancharla, D. Sénéchal, A.-M. S. Tremblay, M. Civelli, and G. Kotliar, Phys. Rev. B **73**, 165114 (2006)] of one-band Hubbard models.
[5] P. Coleman, in *Lectures on the Physics of Highly Correlated Electron Systems VI*, edited by F. Mancini (American Institute of Physics, Melville, NY, 2002), p. 97.
[6] S. Danzenbächer *et al.*, Phys. Rev. Lett. **96**, 106402 (2006).
[7] K. S. Burch, S. V. Dordevic, F. P. Mena, A. B. Kuzmenko, D. van der Marel, J. L. Sarrao, J. R. Jeffries, E. D. Bauer, M. B. Maple, and D. N. Basov, Phys. Rev. B **75**, 054523 (2007).
[8] M. A. Tanatar, J. Paglione, C. Petrovic, and L. Taillefer, Science **316**, 1320 (2007).
[9] N. Doiron-Leyraud, C. Proust, D. Leboeuf, J. Levallois, J. Bonnemaison, R. Liang, D. A. Bonn, W. N. Hardy, and L. Taillefer, Nature (London) **447**, 565 (2007).
[10] E. A. Yelland, J. Singleton, C. H. Mielke, N. Harrison, B. D. F. F. Balakirev, and J. R. Cooper, Phys. Rev. Lett. **100**, 047003 (2008).
[11] A. F. Bangura *et al.*, Phys. Rev. Lett. **100**, 047004 (2008).
[12] S. Doniach, Physica B (Amsterdam) **91**, 231 (1977).
[13] G. Zwicknagl, Adv. Phys. **41**, 203 (1992).
[14] D. L. Cox, *Exotic Kondo Effects in Metals: Magnetic Ions in a Crystalline Electric Field and Tunnelling Centres* (Taylor & Francis, London, 1999).
[15] Y. Shnidman and D. Mukamel, Phys. Rev. B **30**, 384 (1984).
[16] A. J. Millis and P. A. Lee, Phys. Rev. B **35**, 3394 (1987).
[17] H. Ikeda and K. Miyake, J. Phys. Soc. Jpn. **65**, 1769 (1996).
[18] J. Moreno and P. Coleman, Phys. Rev. Lett. **84**, 342 (2000).
[19] P. Ghaemi and T. Senthil, Phys. Rev. B **75**, 144412 (2007).
[20] P. W. Anderson, Phys. Rev. **124**, 41 (1961).
[21] J. R. Schrieffer and P. Wolff, Phys. Rev. **149**, 491 (1966).
[22] B. Coqblin and J. R. Schrieffer, Phys. Rev. **185**, 847 (1969).
[23] J. Kondo, Prog. Theor. Phys. **36**, 429 (1966).
[24] D. Langreth, Phys. Rev. **150**, 516 (1966).
[25] C. M. Varma, Phys. Rev. Lett. **55**, 2723 (1985).
[26] R. K. Kaul, Y. B. Kim, S. Sachdev, and T. Senthil, Nat. Phys. **4**, 28 (2008).
[27] P. A. Lee, Rep. Prog. Phys. **71**, 012501 (2008).
[28] L. Taillefer (private communication).
[29] A. J. Millis and M. Norman, Phys. Rev. B **76**, 220503(R) (2007).
[30] This issue was raised by P. Lee (private communication).
[31] N. Andrei and P. Coleman, Phys. Rev. Lett. **62**, 595 (1989).
[32] T. Senthil, S. Sachdev, and M. Vojta, Phys. Rev. Lett. **90**, 216403 (2003).
[33] M. Dzero and P. Coleman, arXiv:0706.0016, Proceedings of SCES'07, 2007 (unpublished).
[34] P. Coleman, C. Pepin, Q. Si, and R. Ramazashvili, J. Phys.: Condens. Matter **13**, R723 (2001).
[35] T. Senthil, M. Vojta, and S. Sachdev, Phys. Rev. B **69**, 035111 (2004).
[36] Q. Si, S. Rabello, K. Ingersent, and J. L. Smith, Nature (London) **413**, 804 (2001).
[37] T. Senthil, Ann. Phys. **321**, 1669 (2006).
[38] L. E. Ballentine, *Quantum Mechanics: A Modern Development* (World Scientific, Singapore, 2003).